PHYS 410 Project 2

Dora Yang
64828619

December 5, 2022

1 Introduction

In this project we studied numerical methods used to solve partial differential equations (PDEs). Specifically we used the 1-dimensional Crank-Nicholson and the 2-dimensional alternating direction implicit methods to solve Schrödinger's equation. We touch on the properties of numerical solutions to the PDEs such as truncation error and stability. Using the solutions we implemented we carried out convergence analysis and numerical tests to observe how quantum particles interact with different potentials.

2 Background and Theory

2.1 Partial Differential Equations Concepts and Definitions

Partial differential equations (PDEs) are equations that are made up of the partial derivatives of a multi-variable function. They have the following form:

$$\mathbf{L}u = f \tag{1}$$

where $\mathbf{L}$ is a differential operator, u is the solution and f is the source function. This can also be represented as a discrete difference equation:

$$\mathbf{L}^h u^h = f^h \tag{2}$$

where h represents the size of the discretization. In this project we will use discrete approximations of PDEs to determine their numerical solutions.

2.1.1 Residuals

For the exact solution of a PDE the exact solution will have 0 residual. That is:

$$\mathbf{L}^h u^h - f^h = 0.$$

For an approximation $\tilde{u}^h$ to u^h the residual is thus:

$$r^h = \mathbf{L}^h u^h - f^h. \tag{3}$$

2.1.2 Truncation Error

The error between the numerical solution and the exact solution is determined by the error between the differential operator and a difference operator. Thus the truncation error τ^h is:

$$\tau^h = \mathbf{L}^h u - f^h. \tag{4}$$

2.1.3 Convergence

As the discretization size, h, of our numerical method decreases we would expect the numerical solution to converge to the actual solution. Thus, the solution converges if and only if:

$$u^h \to u \text{ as } h \to 0.$$

2.1.4 Consistency

If the truncation error approaches 0 as the discretization size h approaches 0, the numerical method is said the be consistent. This is a necessary condition for convergence.

2.1.5 Accuracy

The numerical method is p^{th} order accurate if:

$$\lim_{h\to 0} \tau^h = O(h^p) \tag{5}$$

2.1.6 Solution Error

The solution error e^h is the difference between the numerical solution and the actual solution of the PDE:

$$e^h = u - u^h. \tag{6}$$

Typically it is assumed that the solution error and truncation error have the same order of magnitude. That is:

$$e^h = \tau^h = O(h^p)$$

2.1.7 Stability

A solution is stable if the size of the solution doesn't change too much with time. We want

$$|u(x,t)| \sim |u(x,0)|$$

for all t.
In general, the solution of a time dependant PDE at t^{n+1} is related to the solution at t^n by an update operater $\mathbf{G}$.

$$u^{n+1} = \mathbf{G}u^n = \mathbf{G}^n u^1, \qquad n = 1, 2...n_{max} \tag{7}$$

Typically when implementing numerical methods to solve PDEs the update operator $\mathbf{G}$ can be represented as a matrix $\underline{\underline{\mathbf{G}}}$. This matrix of course will have a set of eigenvalues μ_j and eigenvectors $\underline{e_j}$ where

$$\underline{\underline{\mathbf{G}}}\,\underline{e_j} = \mu_j \underline{e_j}, \quad j = 1, 2, ...J$$

and

$$u^n = \underline{\underline{\mathbf{G}}}^{n-1} \sum_{j=1}^{J} c_j \underline{e_j} = \sum_{k=1}^{J} c_j \mu_j \underline{e_j} \tag{8}$$

where c_k is a coefficient. The only way the solution does not blow up as n increases is if the eigenvalues μ_k are all less than or equal to 1. For stability we require:

$$|\mu_k| \leq 1. \tag{9}$$

Since update operators typically involve derivatives and difference equations, it is convenient to compute the eigenvalues of the operator $\underline{\mathbf{G}}$ in wave number space rather than real space so that they become algebraic operations. We do this through Fourier analysis. The Fourier Transform of a function $u(x)$ in real space yields a function $\tilde{u}(k)$ in wave space. The Fourier Transform is defined as follows:

$$\tilde{u}^n(k) = \frac{1}{\sqrt{2}\pi} \int_{-\infty}^{\infty} e^{-ikx} u^n(x) dx \tag{10}$$

where k is the wave number and i is the imaginary number. In Fourier space the difference scheme is:

$$\tilde{u}^{n+1}(k) = \underline{\underline{\mathbf{G}}}(\xi) \tilde{u}^n(k). \tag{11}$$

where $\xi = kh$. For stability we still require the magnitude of the eigenvalues of $\underline{\underline{\mathbf{G}}}(\xi)$ to be less than 1. We require $-\pi \leq \xi \leq \pi$.

We will go into more detail about this method when we discuss the stability of different Finite Difference Schemes in sections 2.3.3, 2.3.4 and 2.3.5.

2.2 Schrödinger Equation

In quantum mechanics, Wave-particle duality states that every particle or quantum entity has both particle and wave-like properties. For example electrons in atoms have wave nature that can be described by Schroödinger's equation. The non-dimensionalized Schroödinger equation is given by:

$$i\psi_t = -\nabla^2 \psi + V\psi \tag{12}$$

The Schrödinger equation allows us to determine the wave function ψ of a system. The wave function relates the location of a particle at a given point in space(x, y, z) at a particular time (t) to the wave amplitude. The amplitude of the wave function may be a complex number so it has no real significance. However the square of the wave function $|\psi|^2 = \psi\psi^*$, is the probability (if normalized correctly) of finding an electron at a given point.

2.3 Finite Difference Methods

We will solve the Schrödinger equation using finite difference methods. Finite difference methods are a class of numerical techniques for solving differential equations using finite differences. These methods convert ordinary and partial differential equations into a system of linear equations that can be solved using matrix algebra.
The general process consists of:

1. Discretizing the domain

2. Discretizing the PDE

3. Solve the finite difference scheme

2.3.1 Discretizing the domain

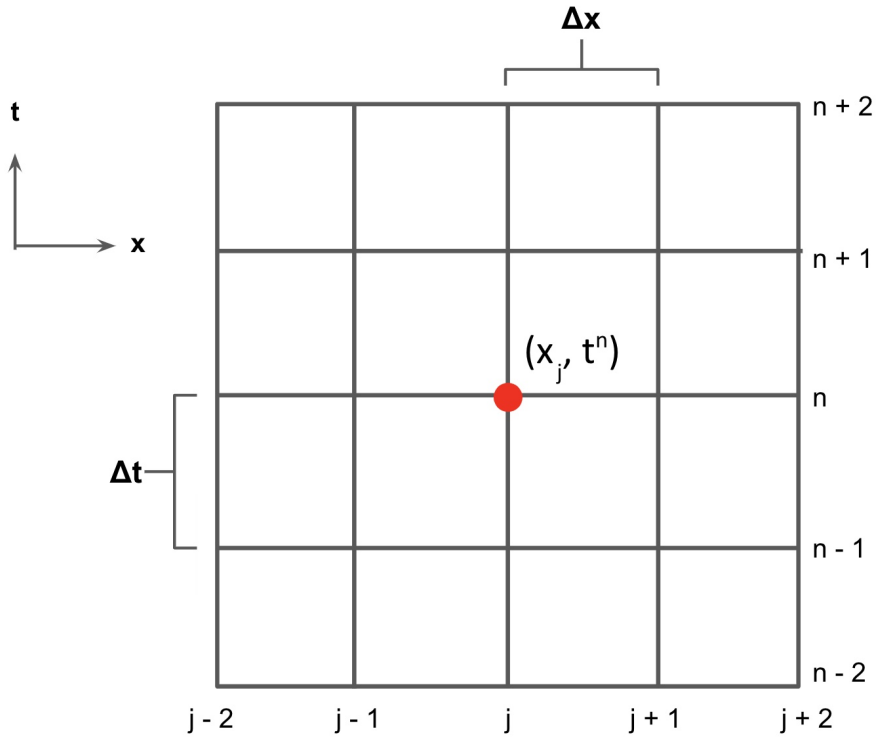

Figure 1: 1D finite difference mesh. The marked point sits at position (x_j, t^n). The spatial dimension has uniform grid spacing Δx and the temporal dimension has uniform grid spacing Δt

To demonstrate this step we will look at the 1-dimensional (in space) case. We replace the continuous time and space values with a uniform mesh. We restrict our domain to $0 \leq x \leq 1$ and $0 \leq t \leq t_{max}$. It is convenient to define the number of grid points using the level integer l where

$$n_x = 2^l + 1,$$

$$\Delta x = \frac{x_{max}}{n_x - 1} = 2^{-l} x_{max},$$

$$x_j = (j-1)\Delta x, \quad j = 1, 2, ...n_x.$$

Both the temporal and spatial direction have uniform grid spacing Δt and Δx respectively. They are related by the ratio $\lambda = \frac{\Delta t}{\Delta x}$. Thus,

$$\Delta t = \lambda \Delta x$$

$$n_t = \frac{t_{max}}{\Delta t} + 1,$$
$$t_n = (n-1)\Delta t, \quad n = 1, 2, ...n_t.$$

The ratio λ is held constant as the size of the grid spacing changes.
For the spatial 2D case a similar mesh will be defind for the unit square domain $0 \leq x \leq 1$, $0 \leq y \leq 1$ and $0 \leq t \leq t_{max}$. Here the spatial grid spacing is equal in both directions $\Delta x = \Delta y$. We will use the grid function notation $\psi^n_{i,j}$ to denote the solution at the point (x_i, y_j, t^n).

2.3.2 Discretizing the PDE

Next, we replace the derivatives in the partial differential equation with difference equations. The Schrödinger equation consists of a first derivative in time and second derivatives in space.

The finite difference approximations (FDAs) are derived from the Taylor series expansions. The derivation of the FDAs and their error was discussed in detail in project 1.

To summarize the results, the forward, backward and central approximation for the first time derivative are given by:

$$\partial_t \psi = \psi_t = \frac{\psi(x, y, t + \Delta t) - \psi(x, y, t)}{\Delta t} = \frac{\psi^{n+1}_{i,j} - \psi^n_{ij}}{\Delta t}, \tag{13}$$

$$\partial_t \psi = \psi_t = \frac{\psi(x, y, t) - \psi(x, y, t - \Delta t)}{\Delta t} = \frac{\psi^n_{i,j} - \psi^{n-1}_{ij}}{\Delta t} \tag{14}$$

and

$$\partial_t \psi = \psi_t = \frac{\psi(x, y, t + \Delta t) - \psi(x, y, t - \Delta t)}{2\Delta t} = \frac{\psi^{n+1}_{i,j} - \psi^{n-1}_{ij}}{2\Delta t} \tag{15}$$

respectively. The FDA for the second derivatives in space is given by

$$\partial_{xx} \psi = \psi_{xx} = \frac{\psi(x + \Delta x, y, t) - 2\psi(x, y, t) + \psi(x - \Delta x, y, t)}{\Delta x^2} = \frac{\psi^n_{i+1,j} - 2\psi^n_{i,j} + \psi^n_{i-1,j}}{\Delta x^2}, \tag{16}$$

and

$$\partial_{yy} \psi = \psi_{yy} = \frac{\psi(x, y + \Delta y, t) - 2\psi(x, y, t) + \psi(x, y - \Delta y, t)}{\Delta y^2} = \frac{\psi^n_{i,j+1} - 2\psi^n_{i,j} + \psi^n_{i,j-1}}{\Delta y^2}. \tag{17}$$

These FDAs have $O(\Delta t), O(\Delta t), O(\Delta t^2), O(\Delta x^2)$ and $O(\Delta y^2)$ error respectively. The overall truncation error of the solution will depend on the finite difference scheme chosen for the analysis. The Crank-Nicholson and Alternating Direction Implicit (ADI) are two finite difference schemes and we will use them to solve the 1D and 2D Schrödinger equations respectively.

2.3.3 Explicit and Implicit Schemes for Solving the 1D Schrodinger Equation

The 1D Schrödinger equation on the domain $0 \leq x \leq 1$ and $\leq t \leq t_{max}$ is given by:

$$i\psi_t = -\psi_{xx} + V(x, t)\psi \tag{18}$$

with the initial and boundary conditions:

$$\psi(x, 0) = \psi_0(x),$$

$$\psi(0,t) = \psi(1,t) = 0.$$

The explicit scheme for solving the Schrödinger involves the forward first time derivative approximation and the 2nd derivative in space. Note the subscript i denotes the i^{th} step in space and should not be confused with the imaginary number i in the Schrödinger equation. Subbing the aforementioned FDAs, equations 13 and 16, into equation 18 we get:

$$i\frac{\psi_i^{n+1} - \psi_i^n}{\Delta t} = -\frac{(\psi_{i+1}^n - 2\psi_i^n + \psi_{i-1}^n)}{\Delta x^2} + V_i^n \psi_i^n \tag{19}$$

which has $O(\Delta t, \Delta x^2)$ truncation error.
Next, using the backwards time derivative approximation, 14, the implicit scheme for solving the Schrödinger equation is given by:

$$i\frac{\psi_i^{n+1} - \psi_i^n}{\Delta t} = -\frac{(\psi_{i+1}^{n+1} - 2\psi_i^{n+1} + \psi_{i-1}^{n+1})}{\Delta x^2} + V_i^{n+1} \psi_i^{n+1}. \tag{20}$$

and also has $O(\Delta t, \Delta x^2)$ truncation error.

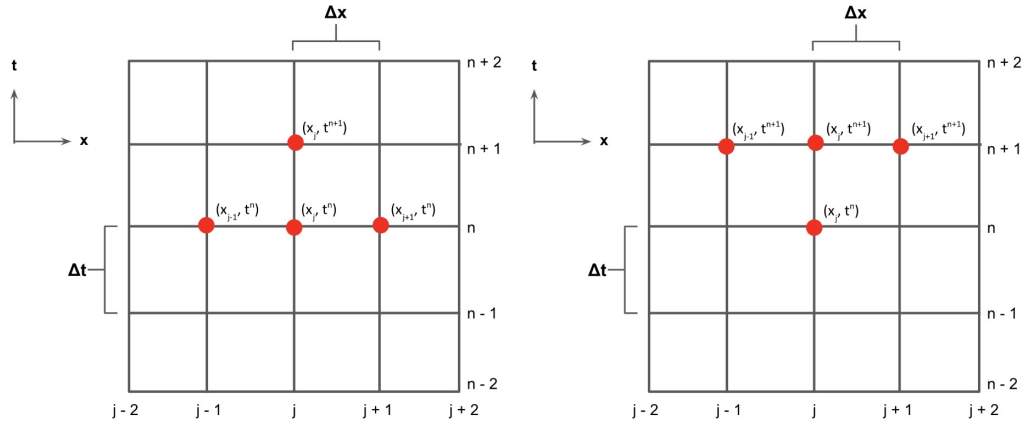

Figure 2: Stencil for explicit (left) and implicit (right) 1D Schrödinger difference equations.

The 2nd scheme is implicit because it has multiple coupled advanced time unknowns as illustrated on the right side of figure 2. The implicit schemes are useful because they tend to be more stable than explicit schemes.

Truncation Error
As previously Discussed, the truncation error for both the explicit and the implicit scheme are $O(\Delta t, \Delta x^2)$. For both, the truncation error is given by:

$$\tau^h = (i\partial_t + \partial_{xx} - V)\psi(x,t)$$

with a Taylor series expansion:

$$\tau^h = i\frac{\Delta t}{2}(\psi_{tt})_j^n + \frac{\Delta x^2}{12}(\psi_{xxxx})_j^n + V + O(\Delta t^2) + O(\Delta x^4) = O(\Delta t, \Delta x^2)$$

Stability

Refer to equations 19 and 20 for the explicit and implicit difference equations. We see that both have a term for the second derivative in space, so let's define a difference operator $\mathbf{D}^2$ where:

$$\mathbf{D}^2\psi = \psi(x+\Delta x) - 2\psi(x) + \psi(x-\Delta x). \tag{21}$$

The Fourier transform of this operator is:

$$\mathbf{D}^2\psi \to -2\sin^2(\frac{\xi}{2})\tilde{u}(k). \tag{22}$$

The explicit and implicit difference equations can be re-written as:

$$\psi^{n+1} = \frac{i\Delta t}{\Delta x^2}\mathbf{D}^2\psi^n + \psi^n,$$

and

$$\psi^{n+1} = \frac{i\Delta t}{\Delta x^2}\mathbf{D}^2\psi^{n+1}\psi^{n+1}.$$

Note, to simplify the notation we've dropped the space subscript i. The potential term is also neglected because we don't have to include potential/undifferentiated terms in Von Neumann stability analysis. In Fourier space the explicit and implicit difference equations are:

$$\tilde{\psi}^{n+1} = (-i\Delta t\frac{4\sin^2(\frac{\xi}{2})}{\Delta x^2} + 1)\tilde{\psi}^n, \tag{23}$$

and

$$\tilde{\psi}^{n+1} = \frac{1}{1 + i\Delta t\frac{4\sin^2(\frac{\xi}{2})}{\Delta x^2}}\tilde{\psi}^n. \tag{24}$$

Recall from section 2.1.7, $\tilde{\psi}^{n+1} = \underline{\underline{\mathbf{G}}}\tilde{\psi}^n$ and the magnitude of the update operator/application factor $|\underline{\underline{\mathbf{G}}}|$ must be less than or equal to 1 for stability. From equations 23 and 24 we see that the explicit scheme will only be stable if $\xi = 0$ and the implicit scheme will always be stable.

2.3.4 Crank-Nicholson Method for solving the 1D Schrödinger equation

The Crank-Nicholson scheme takes and average of the explicit and implicit schemes to make a centered approximation of the time derivative. It is given by:

$$i\frac{\psi_j^{n+1} - \psi_j^{n-1}}{\Delta t} = -\frac{1}{2}(\frac{\psi_{i+1}^{n+1} - 2\psi_i^{n+1} + \psi_{i-1}^{n+1}}{\Delta x^2} + \frac{\psi_{i+1}^{n} - 2\psi_i^{n} + \psi_{i-1}^{n}}{\Delta x^2}) + \frac{1}{2}V_i^{n+1/2}(\psi_i^{n+1} + \psi_i^n) \tag{25}$$

This also improves the accuracy of the solution to $O(\Delta t^2, \Delta x^2)$.

Truncation Error
For the truncation error we take the Taylor expansion of the the interior equation about $(x,t) = (x_j, t^{n+1/2})$:

$$\tau^h = (i\partial_t - \frac{1}{2}(\partial_{xx} + \partial_{xx}) - V)\psi$$

$$\tau^h = \frac{1}{24}\Delta t^2 (u_{ttt})_j^{n+1/2} - \frac{i}{8}\Delta t^2 (u_{ttxx})_j^{n+1/2} - \frac{i}{12}\Delta x^2 (u_{xxxx})_j^{n+1/2} + O(\Delta^4) + O(\Delta x^4) + O(\Delta t^2 \Delta x^2)$$

$$\tau^h = O(\Delta t^2, \Delta x^2)$$

Stability

Using the difference operator $\mathbf{D}^2$, the Crank-Nicholson scheme can be re-written as:

$$(1 - i\frac{\Delta t}{2\Delta x^2}\mathbf{D}^2)\psi^{n+1} = (1 + i\frac{\Delta t}{2\Delta x^2}\mathbf{D}^2)\psi^n,$$

and rearranged in Fourier Space as:

$$\tilde{\psi}^{n+1} = \frac{1 - i\frac{\Delta t}{2\Delta x^2} 4\sin^2(\frac{\xi}{2})}{1 + i\frac{\Delta t}{2\Delta x^2} 4\sin^2(\frac{\xi}{2})}\tilde{\psi}^n.$$

The amplification factor has the form:

$$\frac{1 - ia}{1 + ia}$$

so the magnitude is:

$$|\frac{1 - ia}{1 + ia}| = \sqrt{\frac{1 + a^2}{1 + a^2}} = 1$$

and thus, the Crank-Nicholson scheme is unconditionally stable. Notably because the magnitude will always be 1 this demonstrates the conservation of probability $\int_{-\infty}^{\infty} \psi\psi^*$ exhibited by the solution to the Schrödinger equation.

2.3.5 Alternating Direction Implicit Method for Solving the 2D Schrödinger Equation

The continuous 2D Schrödinger equation on the domain $0 \leq x \leq 1$, $0 \leq y \leq 1$ and $0 \leq t \leq t_{max}$ is given by:

$$\psi_t = i(\psi_{xx} + \psi_{yy}) - iV(x, y)\psi, \tag{26}$$

with the initial and boundary conditions:

$$\psi(x, y, 0) = \psi_0(x, y),$$

$$\psi(0, y, t) = \psi(1, y, t) = \psi(x, 0, t) = \psi(x, 1, t) = 0.$$

The alternating direction implicit (ADI) method is a way to solve the 2D Crank-Nicholson scheme by splitting the compution by the spatial dimensions. The traditonal 2D CN scheme is computionally expensive costing on the order or N^2 operations whereas the ADI scheme costs on the order of N operations. Here, N is the number of edge points on the grid ($N = n_x = n_y$).

For this method we discretize the domain in the same way as the 1D implementation such that:

$$\lambda = \frac{\Delta t}{\Delta x} = \frac{\Delta t}{\Delta y}$$

$$n_x = n_y = 2^l + 1$$

$$\Delta x = \Delta y = 2^{-l}$$

$$\Delta t = \lambda \Delta x$$
$$n_t = \text{round}(\frac{t_{max}}{\Delta t}) + 1$$

The difference equation following the 2D Crank-Nicholson scheme is given by:

$$\frac{1}{\Delta t}(\psi_{i,j}^{n+1} - \psi_{i,j}^{n}) = \frac{i}{2}(\partial_{xx} + \partial_{yy})(\psi_{i,j}^{n+1} + \psi_{i,j}^{n}) - \frac{i}{2}V(\psi_{i,j}^{n+1} + \psi_{i,j}^{n}) \tag{27}$$
$$i = 2, 3, ...n_x - 1, j = 2, 3, ..., n_y - 1, n = 1, 2, ...n_t - 1$$

For this analysis we assume that the Crank-Nicholson scheme retains it's nice properties from the 1D version in that it is unconditionally stable, conserves probability and has $O(\Delta^2, \Delta x^2)$ truncation error. We define the differential operator $\mathbf{L}^h$:

$$\mathbf{L} = \partial_{xx}^h + \partial_{yy}^h.$$

To implement the ADI scheme we want to factor the operators in the Crank-Nicholson scheme into a product of 1D operators so that they can be solved sequentially. Doing so yields:

$$(1 - i\frac{\Delta t}{2}\partial_{xx}^h)(1 - i\frac{\Delta t}{2}\partial_{yy}^h + i\frac{\Delta t}{2}V_{i,j})\psi_{i,j}^{n+1} = (1 + i\frac{\Delta t}{2}\partial_{xx}^h)(1 + i\frac{\Delta t}{2}\partial_{yy}^h - i\frac{\Delta t}{2}V_{i,j})\psi_{i,j}^{n}. \tag{28}$$

Since we only require $O(\Delta t^2, \Delta x^2)$ accuracy, extra terms such as $\frac{\Delta t^2}{2}\partial_{xx}^h\partial_{yy}^h(\psi_{i,j}^{n+1} - \psi_{i,j}^{n})$ are neglected because they become $O(\Delta t^3)$ when we take the Taylor series expansion of the difference equation.

Computationally we solve the ADI scheme in two steps:

$$(1 - i\frac{\Delta t}{2}\partial_{xx}^h)\psi_{i,j}^{n+1/2} = (1 + i\frac{\Delta t}{2}\partial_{xx}^h)(1 + i\frac{\Delta t}{2}\partial_{yy}^h - i\frac{\Delta t}{2}V_{i,j})\psi_{i,j}^{n}, \tag{29}$$

and then:

$$(1 - \frac{\Delta t}{2}\partial_{yy}^h + i\frac{\Delta t}{2}V_{i,j})\psi_{i,j}^{n+1} = \psi_{i,j}^{n+1/2}. \tag{30}$$

3 Implementation

3.1 Files

This project was completed using Matlab. The key files and their descriptions are listed in table 1

Table 1: Project files and descriptions

File	Description
sch_1d_cn.m	Function for computing the 1D Crank-Nicolson solution to Schrödinger's equation.
ctest_1d.m	Script that runs a 4-level convergence test and an exact error test for sch_1d_cn.m. See section 4.1 for discussion.
barrier_survey.m	Script that runs a survey to plot the excess fractional probability of a quantum particle beyond a barrier of varying potential. See section 4.2.1 for discussion.
well_survey.m	Script that runs a survey to plot the excess fractional probability of a quantum particle within a well of varying potential. See section 4.2.2 for discussion.
sch_2d_adi.m	Function for computing the 2D ADI solution to Schrödinger's equation.
ctest_2d.m	Script that runs a 4-level convergence test and an exact error test for sch_2d_cn.m. See section 4.1 for discussion.
sch_2d_videos.m	Script for defining the required parameters and running the simulations associated with the 2D numerical experiment videos.
video_generator.m	Function for generating videos given the solution from the 2D ADI implementation.
Gaussian_barrier.avi	Video of 2D boosted Gaussian and potential barrier simulation discussed in section 4.4.1
Gaussian_well_trapped.avi	Video of 2D boosted Gaussian stuck inside a box simulation discussed in section 4.4.2
Gaussian_well_small.avi	Video of 2D boosted Gaussian and small potential ($V = -10^2$) discussed in section 4.4.2
Gaussian_well_big.avi	Video of 2D boosted Gaussian and small potential ($V = -10^8$) discussed in section 4.4.2
Gaussian_well_medium.avi	Video of 2D boosted Gaussian and small potential ($V = -10^5$) discussed in section 4.4.2
Double_slit.avi	Video of double slit simulation discussed in section 4.4.3
Double_slit_interference.avi	Video of double slit interference with source wave omitted to emphasis the interference pattern
Figures	Folder containing figures and plots used in this report.

3.2 Implementation of 1D Crank-Nicholson Method

The sch_1d_cn.m function computes the 1D Crank-Nicholson solution to Schrödinger's equation and returns time and position vectors corresponding to the grid points of the solution ψ. ψ is also returned and it is represented as a 2D array where the rows correspond to the time steps $t = 0, \Delta t, 2\Delta t, 3\Delta t, ..., t_{max}$ and the columns represent the x positions $x = 0, \Delta x, 2\Delta x, 3\Delta x, ..., 1$.

Our end goal is to populate the solution matrix for all time and points in space starting with the chosen initial condition. We loop through the time elements and update the solution in accordance

to equation 25. Grouping $n+1$ and n terms to the left and right of the equality we get:

$$\begin{aligned}\frac{1}{2\Delta x^2}\psi_{i+1}^{n+1} + (\frac{i}{\Delta t} - \frac{1}{\Delta x^2} - \frac{1}{2}V_i^{n+1})\psi_i^{n+1} + \frac{1}{2*\Delta x^2}\psi_{i-1}^{n+1} = \\ -\frac{1}{2\Delta x^2}\psi_{i+1}^{n} + (\frac{i}{\Delta t} + \frac{1}{\Delta x^2} + \frac{1}{2}V_i^{n+1})\psi_i^{n+1} - \frac{1}{2*\Delta x^2}\psi_{i-1}^{n}\end{aligned} \tag{31}$$

On the right hand side of the equations all of the quantities are known so they can be directly computed and stored in a temporary vector f. For the left hand side, we set up a matrix A using the coefficients for the different spatial elements for the $n+1$ time step. Since this equation only depends on the 3 spatial points $i, i+1$ and $i-1$ we can use Matlabs spdiags feature to define a tri-diagonal matrix with the 3 coefficients needed rather than a full matrix with a bunch of zeroes. This is computationally much more efficient reducing the number of operations needed. The solution for the next time step ψ^{n+1} is computed using Matlab's left-division function:

$$\psi^{n+1} = A \setminus f.$$

3.3 Implementation of 2D ADI Method

The sch_1d_cn.m function computes the 1D Crank-Nicholson solution to Schrödinger's equation and returns time and position vectors corresponding to the grid points of the solution ψ. ψ is also returned and it is represented as a 3D matrix where time is the first dimension, x is the second dimension and y is the third dimension.

Like with the 1D case, we want to populate the solution matrix for all time and points in space starting with the chosen initial condition. We loop through the time elements and update the solution in accordance to equations 29 and 30. This consists of doing 2 left divisions sequentially one corresponding to each of the aforementioned equations.

4 Analysis and Results

4.1 1D Convergence Testing

Convergence testing allows us to study the behaviour of the solution as the size of the time and spatial steps Δt and Δx tend to 0, otherwise as the discretization level increases. One way to do convergence testing is taking the level to level differences between 2 sets of solutions such that:

$$d\psi^l = \psi^{l+1} - \psi^l. \tag{32}$$

We can compute the magnitude of the difference at each time step to get:

$$||d\psi^l||_2(t^n), \tag{33}$$

where:

$$||d\psi^l||_2(t^n) = \sqrt{\frac{\sum_{i=1}^{n_x}|\psi(x_i,t^n)|^2}{n_x}}. \tag{34}$$

As previously discussed the Crank-Nicholson method is $O(h^2)$ accurate (where $h = \Delta x = \frac{\lambda}{\Delta t}$). Since we know our numerical method is second order accurate we can expect that if the level to level differences of adjacent levels will coincide if the higher level is scaled by a factor of $\rho = 4$, that is:

$$d\psi^{l_0} = 4d\psi^{l_0+1} = 4^2 d\psi^{l_0+2} = 4^3 d\psi^{l_0+3} = ... = 4^n \psi^{l_0+n}. \tag{35}$$

The script ctest_1d.m implements and plots a 4 level convergence test for 2 sets of system parameters.

Table 2: 1D Convergence Test Parameters, Case 1

Parameter	**Value**
Initial Condition	$\psi(x,0) = \sin(3\pi x)$
Potential	None
Levels	$l_{min} = 6$, $l_{max} = 9$
λ	0.5
t_{max}	0.25
Exact Solution	$e^{-i(3^2)\pi^2 t}\sin(2\pi x)$

Table 3: 1D Convergence Test Parameters, Case 2

Parameter	**Value**
Initial Condition	$\psi(x,0) = e^{-((x-0.5)/0.075))^2}$
Potential	None
Levels	$l_{min} = 6$, $l_{max} = 9$
λ	0.01
t_{max}	0.25

In figures 3 and 4 we've plotted the level to level differences scaled in accordance to equation 35. In both cases, there is near coincidence of the lines demonstrating that our simulation does have second order accuracy as expected. In figure 4 it can be noted that the lowest level line does not perfectly line up with the others suggesting that the solution may not have converged yet. We repeated the case 2 convergence test this time using levels 7 to 10 and plotted the results in figure 5 and observed better alignment of the lines which demonstrates convergence.

For case 1, the initial condition $\psi(x,0) = \sin(3\pi x)$ yields an exact solution $\psi_{exact}(x,t) = e^{-i3^2\pi^2 t}\sin(3\pi x)$. Similar to the level to level difference, we can compute the exact error to be:

$$||E(\psi^l)||_2(t^n) = ||\psi_{exact} - \psi^l)||_2(t^n) \tag{36}$$

We can also plot the exact errors for each level following the same scaling scheme as before. This was done in figure 6. Again, the error lines coincided for $\rho = 4$ demonstrating that the solution error is also second order accurate. The confirms the statement in section 2.1.6 that the solution error and truncation error are typically the same order of magnitude.

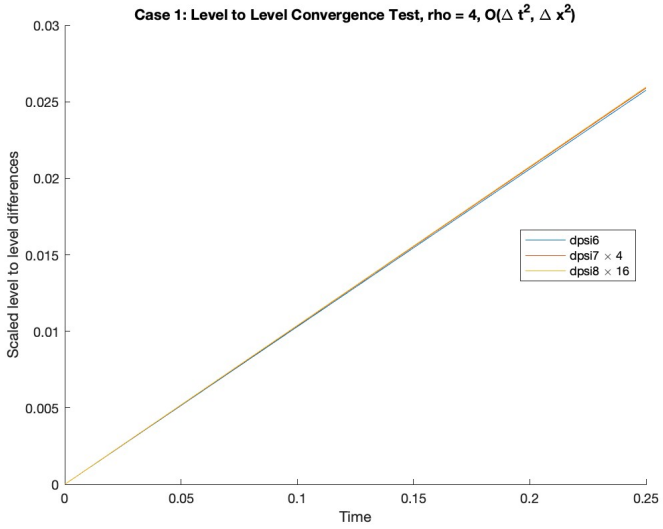

Figure 3: Level to level convergence test for 1D Schrödinger equation solved by the Crank-Nicholson method using case 1 parameters. Coincidence of plots scaled by $\rho = 4$ demonstrate the second order accuracy of the scheme.

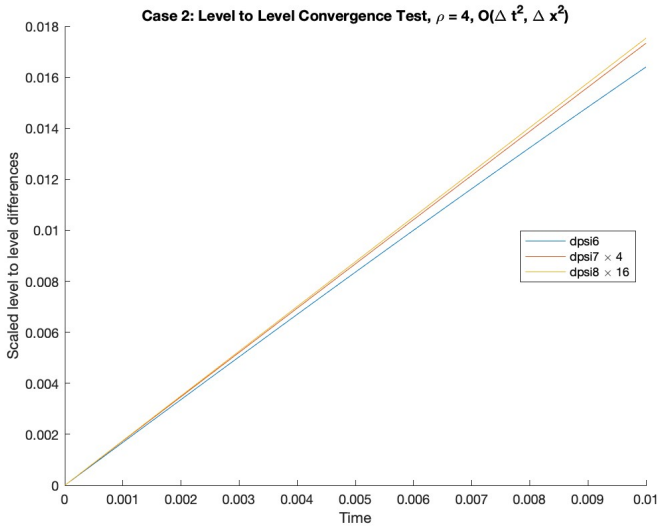

Figure 4: Level to level convergence test for 1D Schrödinger equation solved by the Crank-Nicholson method using case 2 parameters. Coincidence of plots scaled by $\rho = 4$ demonstrate the second order accuracy of the scheme.

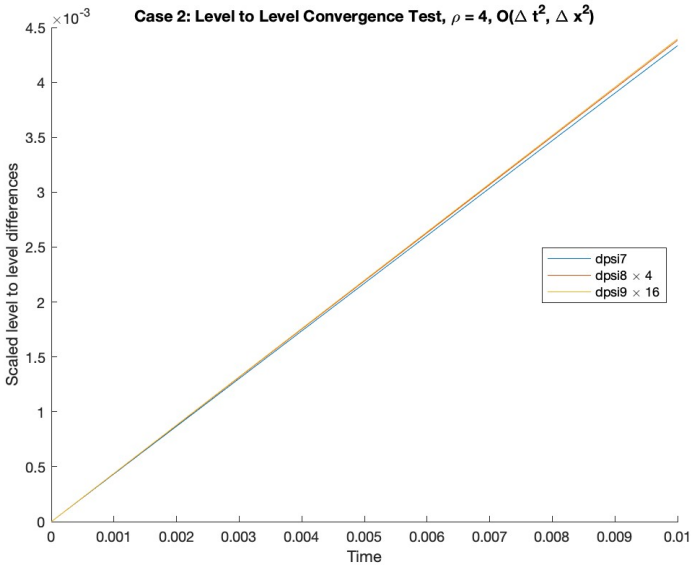

Figure 5: Level to level convergence test for 1D Schrödinger equation solved by the Crank-Nicholson method using case 2 parameters. Increased level from 6-9 to 7-10 to demonstrate convergence with smaller time and spatial steps.

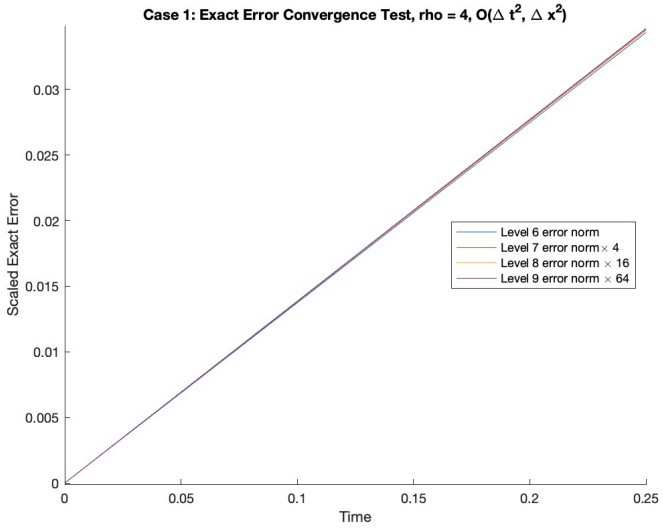

Figure 6: Exact error convergence test for parameter set 1. The solution error is second order.

4.2 1D Numerical Experiments: Potentials and Probability Distributions

As briefly touched up in section 2.2, the probability density of the solution to the Schrödinger equation $\rho = |\psi|^2 = \psi\psi^*$. We define $P(x,t)$ as the running integral of this quantity:

$$P(x,t) = \int_0^x \psi(\tilde{x},t)\psi^*(\tilde{x},t)d\tilde{x}, \tag{37}$$

and $P(1,t) = 1$ if the wavefunction is properly normalized. Essentially $P(a,t)$ is the probability of finding the "particle" between $x = 0$ and $x = a$. In grid notation, $P_i^n = P(x_i, t^n)$ for $i = 1, 2, ...n_x$ and $n = 1, 2, ...n_t$. We define the temporal average of the running integral of the probability density to be:

$$\bar{P}_i = \frac{\sum_{n=1}^{n_t} P_i^n}{n_t}, \tag{38}$$

essentially the average of P_i for all time steps. Since we want this to be normalized so that $\bar{P}_{n_x} = 1$ we set:

$$\bar{P}_i := \frac{\bar{P}_i}{\bar{P}_{n_x}}. \tag{39}$$

Thus, given that $x_2 > x_1$ $\bar{P}(x_2) - \bar{P}(x_1)$ represents the fraction of time the quantum particle spends in the interval $x_1 \leq x \leq x_2$. In the case of a free particle, the potential V = 0 for all space and for sufficiently long times, we would observe that:

$$\bar{P}(x_2) - \bar{P}(x_1) \to x_2 - x_1.$$

With a non-zero potential, the excess fractional probability tells us the fraction of time a particle spends in an interval compared to the same interval in free space. It is defined as:

$$\bar{Fe}(x_1, x_2) = \frac{\bar{P}(x_2) - \bar{P}(x_1)}{x_2 - x_1}. \tag{40}$$

Since $\bar{Fe}(x_1, x_2)$ can span orders of magnitudes for different potentials it is convenient to compute and plot the natural log:

$$\ln \bar{Fe}(x_1, x_2) = \ln \frac{\bar{P}(x_2) - \bar{P}(x_1)}{x_2 - x_1}. \tag{41}$$

For this section of the analysis we ran 2 numerical surveys to observe the behaviour of the particle under different potential distributions a barrier and a well. The 2 surveys shared the following parameters: $t_{max} = 0.1$, level = 9, $\lambda = 0.01$, a boosted Gaussian initial condition and a constant potential V_0 in the range $0.6 \leq x \leq 0.8$.

4.2.1 Barrier Survey

For this survey (script barrier_survey.m) we considered a barrier of height V_0, we varied the magnitude of the potential so that:

$$-2 \leq \ln(V_0) \leq 5 \to e^{-2} \leq V_0 \leq e^5.$$

The potential was constant and equal to V_0 in the range $0.6 \leq x \leq 0.8$ and 0 elsewhere, as depicted in figure 9. The specific boosted Gaussian initial condition used was $\psi(x,0) = e^{i20t}e^{-((x-0.4)/0.075)^2}$

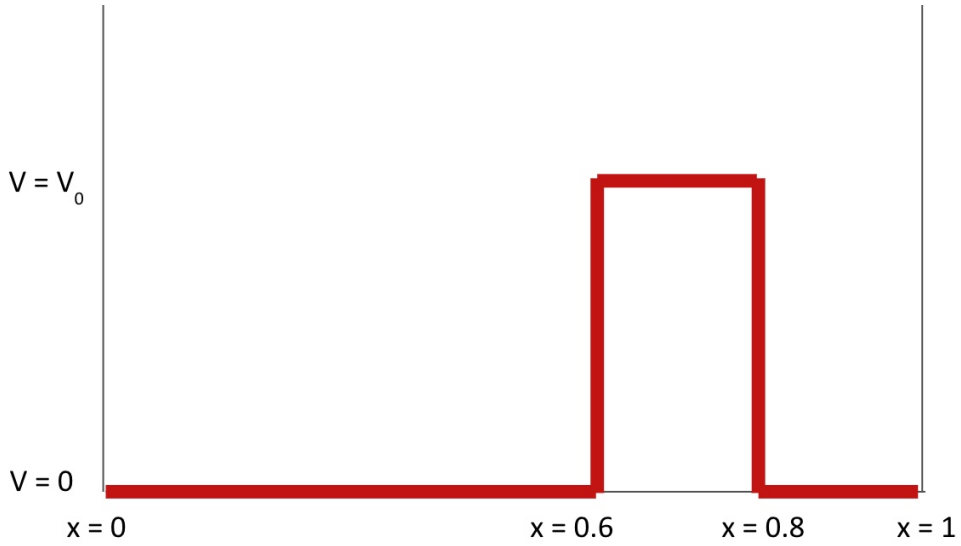

Figure 7: Barrier potential plot. A constant positive potential V_0 exists between $0.6 \leq x \leq 0.8$ and the potential is 0 elsewhere.

so that the particle start to the left of the barrier. We are interested in the likely hood of a particle existing in the region to the right of the barrier so we will compute the excess fractional probability in the range $0.8 \leq x \leq 1.0$, $\bar{Fe}(0.8, 0.1)$.

In figure 8 we plotted $\ln(\bar{Fe}(0.8, 0.1)$ as a function of $\ln(V_0)$. From these results we can make several observations about the behaviour of a quantum particle near a barrier. First, we see that between $\ln(V_0) = -2$ and $\ln(V_0) = 2\ln(\bar{Fe})$ is approximately equal to 0. As such in that range $\bar{Fe}(0.8, 1.0)$ is approximately equal to 1. We interpret that as for potential barriers between $V_0 = e^{-2}$ and $V_0 = e^2$ the particle is able to go beyond the barrier just as often as it would in free space. This likely means that in this case the particle has more energy than the potential barrier. From this point onward, $\ln(\bar{Fe})$ begins to rapidly decrease. Now, for a classical particle if the energy of the particle was less than the potential barrier then it would not pass through at all and $\bar{Fe}(0.8, 1.0)$ would be equal to 0 for all $V_0 > E_{particle}$ we would see $\ln(Fe) \to -\infty$. Of course we take quantum effects such as tunneling into account. Quantum tunneling refers to the phenomenon where part of a wave-function can propagate through a higher energy potential barrier explaining why $\bar{Fe}(0.8, 1.0)$ is non-zero for large potentials. Of course we still observe a rapid drop in $\ln(\bar{Fe}(0.8, 1.0))$ because as the potential barrier increases, the probability/amount of quantum tunneling decreases.

4.2.2 Well Survey

For the well survey (script well_survey.m) we considered negative potentials. Meaning we varied the depth of a well with potential $V_0 < 0$. We varied the magnitude so that:

$$2 \leq \ln(|V_0|) \leq 10 \to e^2 \leq |V_0| \leq e^{10}.$$

The potential was constant and equal to V_0 in the range $0.6 \leq x \leq 0.8$ and 0 elsewhere, as depicted in figure 9. The specific boosted Gaussian initial condition used was $\psi(x, 0) = e^{-((x-0.4)/0.075)^2}$.

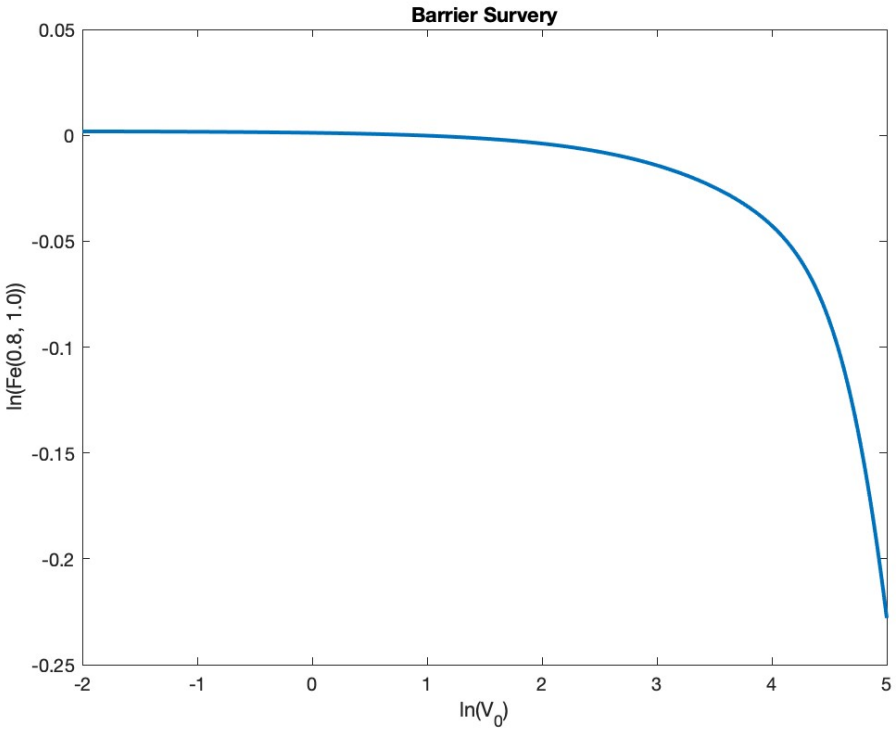

Figure 8: Barrier potential survey.

This time we measured $\bar{Fe}(0.6, 0.8)$ which is the excess fractional probability of the quantum particle being in the well.

The results of the well survey are plotted in figure 10. Here are some observations that can be made from the results of the survey. A quantum particle can interact with a potential well through transmission, scattering and trapping. We first notice that between $|\ln(V_0)| = 2$ and $|\ln(V_0)| = 4$ $\ln(\bar{Fe}(0.6, 0.8))$ is approximately 0 and for some portions even greater than 0. This means for these lower potential wells the quantum particle spends more time in the well than it would in that region in free space. This behaviour is somewhat analogous to the classical case where the particle would "fall into" and stay in the region of lower potential. We observe that as the depth of the potential well increases, it appears that $\ln(\bar{Fe}(0.6, 0.8))$ tends to decrease. Of course there are multiple thin spikes in $\ln(\bar{Fe}(0.6, 0.8))$ which can likely be explained by quantum bound states. For finite potential wells there are specific bound states where particles are more likely to get trapped in the well. These bound states relate to the energy of the particle and the potential of the well meaning only certain quantum particles with discrete energies E_n will have a high likely hood of being trapped in the well. A classical analogy would be like only certain wavelengths of light forming standing waves in a cavity. The spikes we see happen at the potentials with V_0 proportional to the energy of the particle (determined by the initial condition). For extremely large potential wells there won't be any penetration through the well at all which is why the fractional probability is so low.

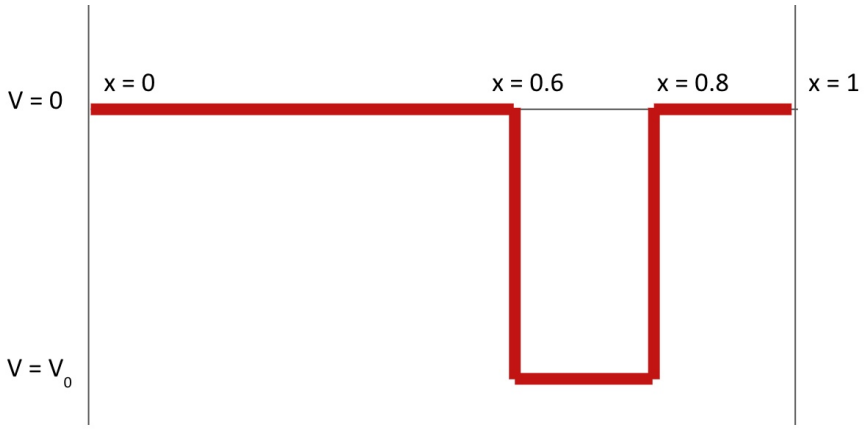

Figure 9: Well potential plot. A constant negativepotential V_0 exists between $0.6 \leq x \leq 0.8$ and the potential is 0 elsewhere.

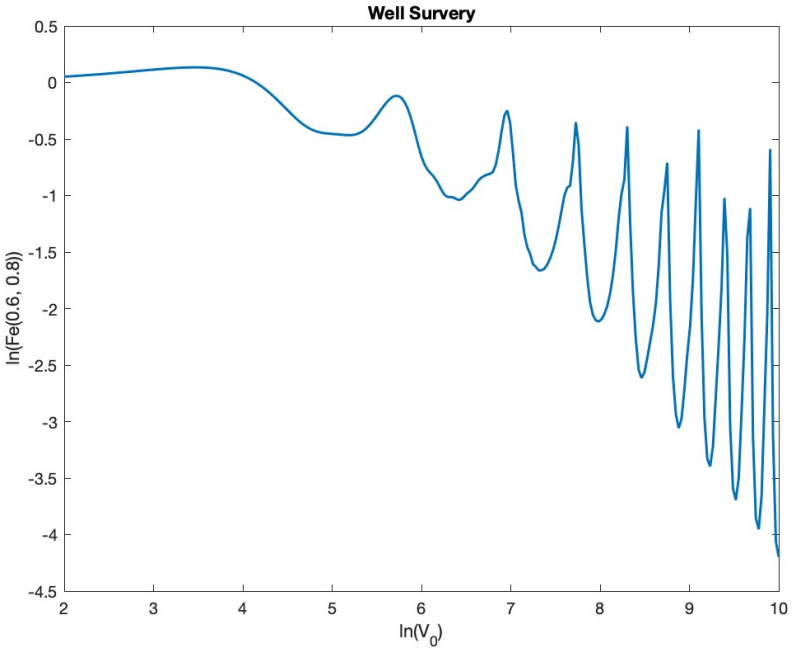

Figure 10: Well potential survey.

4.3 2D Convergence Testing

For 2D convergence testing we follow the exact same procedure as the 1D test outlined in section 4.1. The only difference is that the norms $||d\psi^l||$ and $||E(\psi^l)||$ consist of the sum over both spatial dimensions for a given time t^n.

We performed the level to level and exact error convergence test for the same set of parameters. That is, $\psi(x, y, 0) = \sin(2\pi x)\sin(3\pi y)$, $l_{min} = 6$, $l_{max} = 9$, $t_{max} = 0.05$

Table 4: 2D Convergence Test Parameters

Parameter	**Value**
Initial Condition	$\psi(x, y, 0) = \sin(2\pi x)\sin(3\pi y)$
Potential	None
Levels	$l_{min} = 6$, $l_{max} = 9$
λ	0.05
t_{max}	0.05
Exact Solution	$e^{-i(2^2+3^2)\pi^2 t}\sin(2\pi x)\sin(3\pi y)$

As discussed in section 2.3.5, the 2D ADI solver is 2nd order accurate, thus like the 1D Crank-Nicholson method scaling the level to level differences and exact errors by a factor $\rho = 4$ should give near coincidence of the plots. This is exactly what we observe in figures 11 and 12 confirming that our implementation is 2nd order accurate as expected.

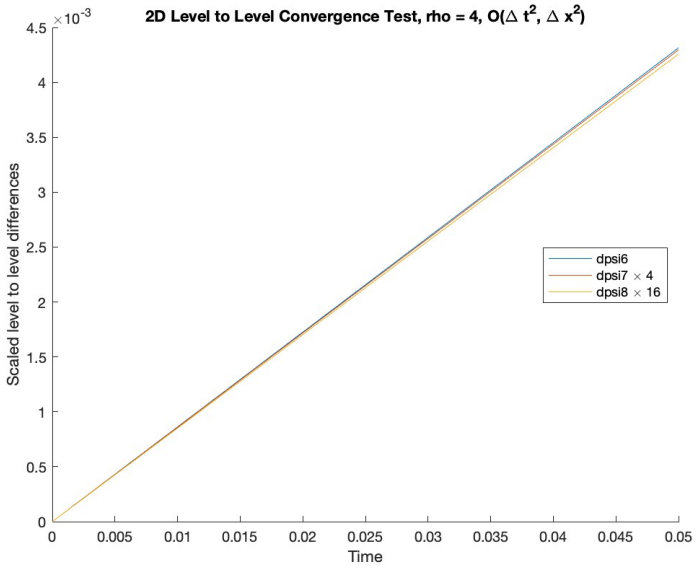

Figure 11: Level to level convergence test for 2D Schrödinger equation solved by the ADI. Coincidence of plots scaled by $\rho = 4$ demonstrate the second order accuracy of the scheme.

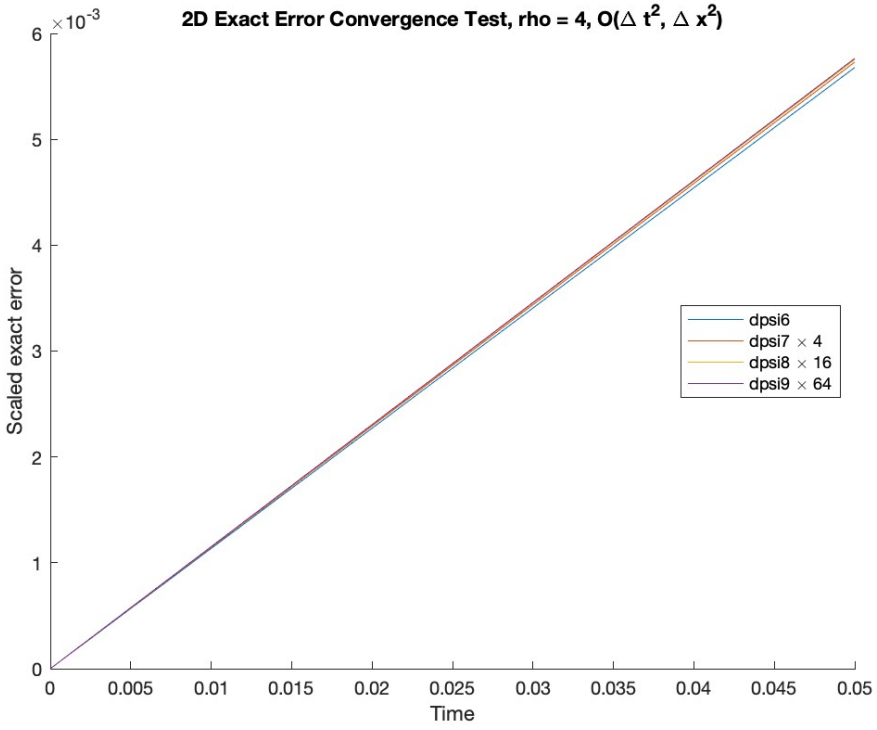

Figure 12: Exact error convergence test for 2D Schrödinger equation solved by the ADI. Coincidence of plots scaled by $\rho = 4$ demonstrate the second order accuracy of the scheme.

4.4 2D Numerical Experiments

Using our ADI implementation of the 2D Schrödinger equation we completed several numerical experiments to demonstrate how the wave function interacts with different types of potentials. We created videos (listed with descriptions in table 1). We stitched together the surface plots of the modulus of the solution ψ at each time t for $t = t_1, t_2, ..., t_{max}$ to form the frames that make up the videos. Recall that the modulus

$$\rho = \sqrt{\psi\psi^*}$$

where ψ^* is the complex conjugate of ψ. The modulus (when the function is correctly normalized) represents the probability of a quantum particle being at a certain spot at a given time. For our purposes we did not normalize since we weren't looking for the exact probabilities. Instead, creating a surface plot with colours that varied according to the magnitude of the modulus was sufficient for demonstrating the behaviour of the wave function with different potentials.

For all these tests we used at boosted Gaussian initial condition which has the form:

$$\psi(x, y, 0) = e^{ip_x x} e^{ip_y y} e^{-((x-x_0)^2/\delta_x^2 + (y-y_0)^2/\delta_y^2)} \tag{42}$$

where the parameters x_0 and y_0 are the initial positions of the center of the Gaussian distribution, δ_x and δ_y correspond to the x and y width of the distribution and p_{xx} and p_{yy} relate to the initial

momentum/speed of the distribution in the x and y directions respectively.

4.4.1 Rectangular Barrier

First, we simulated how the wave function would interact with a potential barrier. The parameters for the simulation are listed in table 8. The frames from the video *gaussian_barrier.avi* can be seen in figures 13 and 14. In figure 13 we first see the initial distribution of the right and on the left we see how the Gaussian has travelled towards the potential (due to the initial momentum given). Here we see that $\sqrt{\psi\psi^*}$ is still 0 inside the potential barrier. We observe the same at a later timestep in figure 14. This behaviour is the same as the 1D case discussed in section 4.2.1. The initial wave-function distribution has some associated energy but because the potential of the barrier is higher (many orders of magnitude) there is 0 probability that the quantum particle will find itself inside the region of the potential barrier.

Table 5: 2D Rectangular Barrier Potential Experiment Parameters

Parameter	**Value**
Initial Condition	$\psi(x,y,0) = e^{i100x}e^{i100y}e^{-((x-0.3)^2/0.08^2+(y-0.3)^2/0.08^2)}$
Potential	Rectangular barrier. $V = 10^8$, $0.5 \leq x \leq 0.7$, $0.5 \leq x \leq 0.7$
Level	9
λ	0.01
t_{max}	0.003

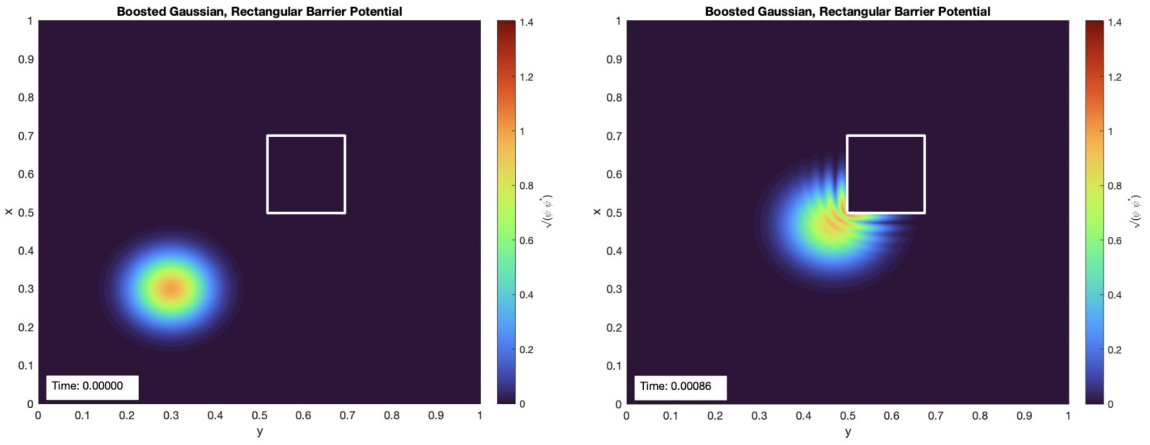

Figure 13: Surface plot of $\sqrt{\psi\psi^*}$ interacting with a rectangular barrier potential (bounds outlined in white) at $t = 0, n = 1$ (right) and $t = 0.00086, n = 44$ (left).

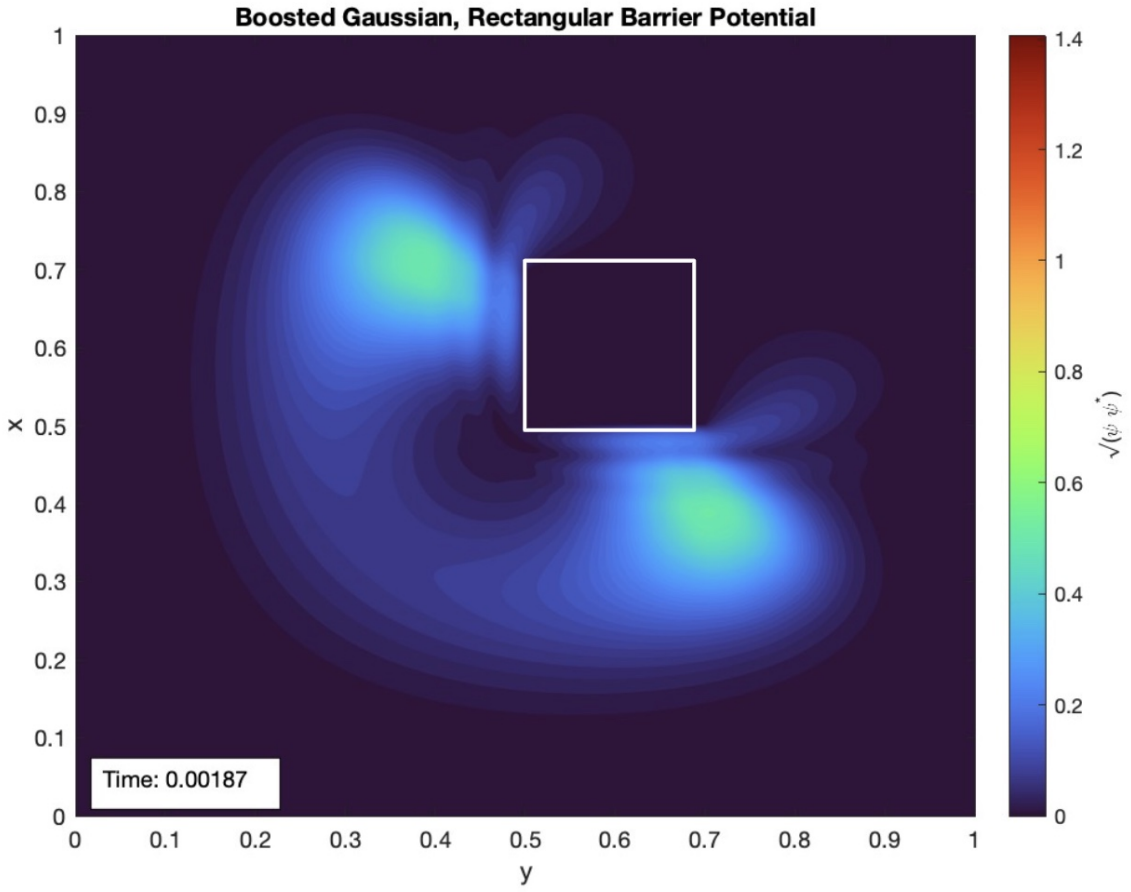

Figure 14: Surface plot of $\sqrt{\psi\psi^*}$ interacting with a rectangular barrier potential (bounds outlined in white) at $t = 0.00187, n = 97$.

4.4.2 Rectangular Well

Next we looked at how the wavefunction might interact with a negative potential well. First, we looked at the case where the quantum particle is inside the potential well. This is analogous to the particle in a box model. This experiment can be viewed in the video *Gaussian_well_trapped.avi*.

Table 6: 2D Particle Trapped in a Well Parameters

Parameter	**Value**
Initial Condition	$\psi(x, y, 0) = e^{-((x-0.5)^2/0.08^2+(y-0.5)^2/0.08^2)}$
Potential	Rectangular Well $V = -10^4$ $0.3 \leq x \leq 0.7$, $0.3 \leq y \leq 0.7$
Level	9
λ	0.01
t_{max}	0.02

We start with a Gaussian centered at $x = 0.5$ and $y = 0.5$ with no initial speed/momentum. As time progresses, $\sqrt{\psi\psi^*}$ oscillates into different probability distributions. In a classical system a particle trapped in a box is no more likely to be found at one position over another. In a quantum system the particle may only occupy certain energy levels (related to the geometry and potential of the box) meaning it may be more likely to occupy certain positions in the box. If that was the case we would observe that for large t the distribution of $\sqrt{\psi\psi^*}$ would remain relatively constant. We were unable to observe this behaviour because due to difficulties in finding initial conditions and potential parameters to get the correct bound state energies.

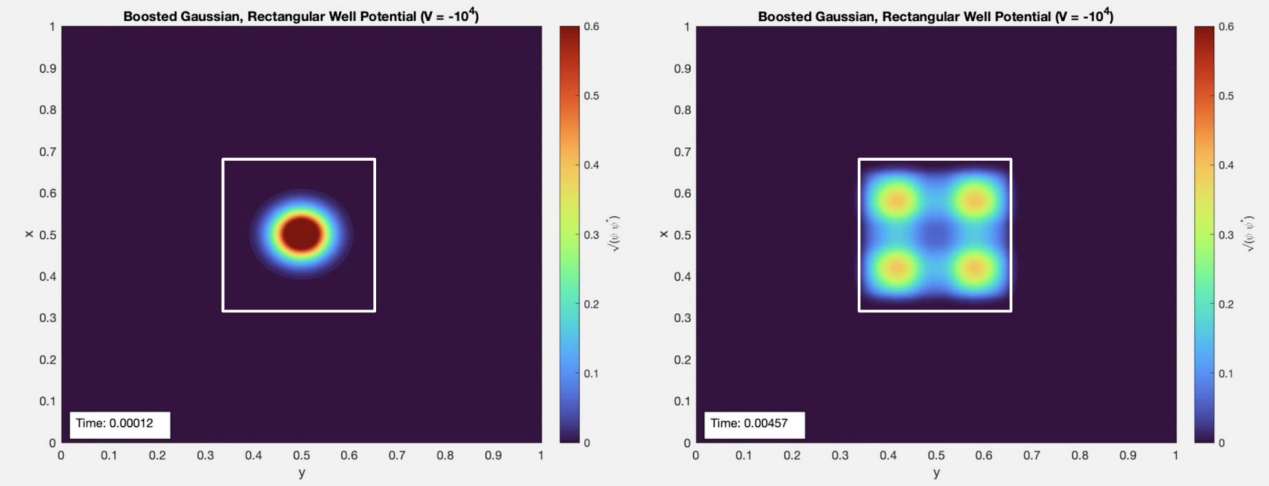

Figure 15: Quantum particle trapped in a well.

Next, we considered a how a particle outside of a well might interact with it. We looked at 3 different magnitudes and placed the potential right next to the boundary to try to negate any boundary condition effects.

Table 7: 2D Particle Outside a Well Parameters

Parameter	**Value**
Initial Condition	$\psi(x, y, 0) = e^{i100y} e^{-((x-0.5)^2/0.08^2 + (y-0.7)^2/0.08^2)}$
Potential	Rectangular Well $V = -10^2, -10^5, -10^8$ $0.3 \leq x \leq 0.7$, $0.8 \leq y \leq 0.99$
Level	9
λ	0.01
t_{max}	0.02

First we considered the case with a small potential $V = -10^2$ in the video *Gaussian_well_small.avi* and figure 16. We observed that wave distribution spread as if there was no potential at all. Next we considered the case with a very large negative potential $V = -10^8$ in the video *Gaussian_well_big.avi* and figure 17. We observed that the particle does not enter the well at all similar to what we saw in the 1D case discussed in section 4.2.2. Finally we considered an intermediate potential $V = -10^5$

in the video *Gaussian_well_medium.avi* and figure 18 and observed that some of the distribution entered the well and some did not. The interpretation of this is that there is a non-zero probability that the quantum particle can enter the well not 0% as with the classical case.

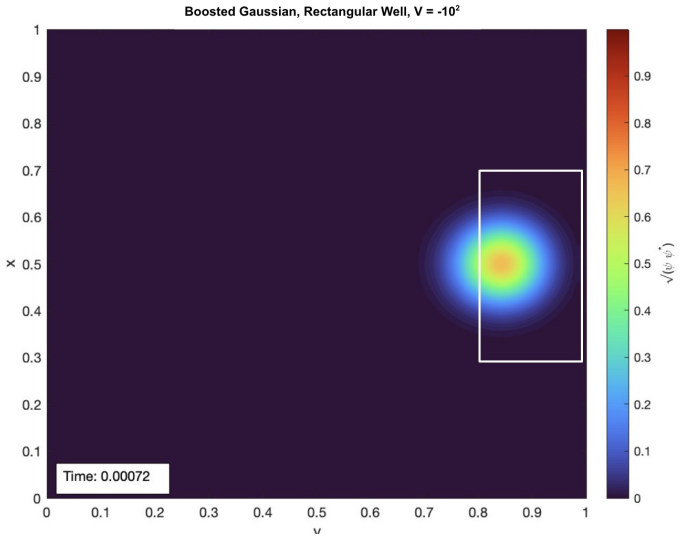

Figure 16: Small well potential ($V = -10^2$), particle behaves as if it were in free space.

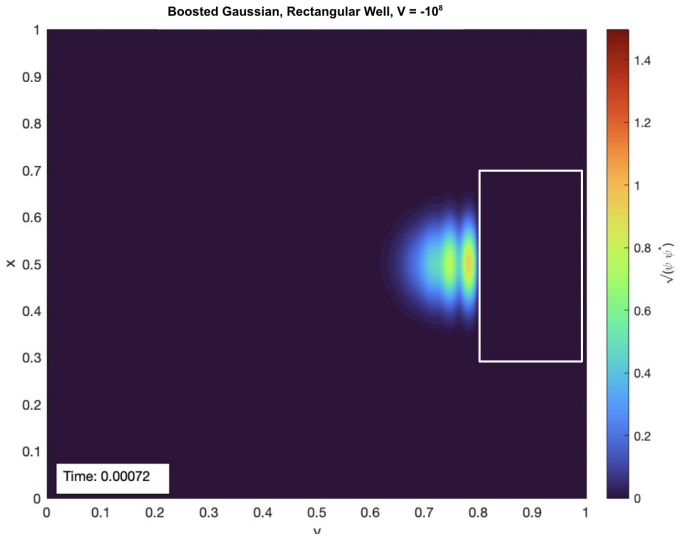

Figure 17: Big well potential (($V = -10^8$), particle behaves as if there were a potential barrier.

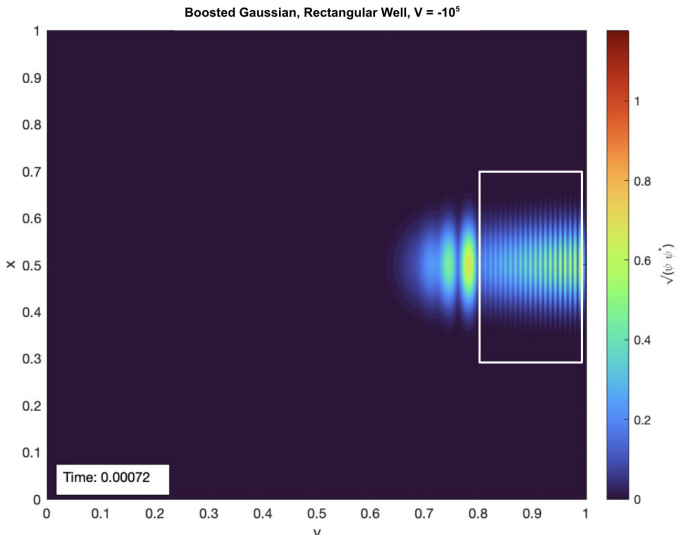

Figure 18: Intermediate well potential ($V = -10^5$), some of the $\sqrt{\psi\psi^*}$ distribution enters the well some of it is reflected.

4.4.3 Double Slit

Theory
Before we discuss the results of the simulation we'll provide some theory and context about double slit experiment. This experiment demonstrated the wave and particle in of light. In quantum mechanics Wave-particle duality is a concept that says quantum particles may be described as either a particle or a wave, but neither classical concept can fully describe this behaviour in isolation. At a high level, a plane light wave is split in to 2 sources when it hits a barrier with 2 slits. The resulting waves form an interference pattern with alternating dark and bright spots due to the difference in wave path lengths. This interpretation in demonstrated in figure 19. More notably, this result/interference pattern has been reproduced in experiments where single photons are sent through the double slit at a time demonstrating their wave-particle duality.

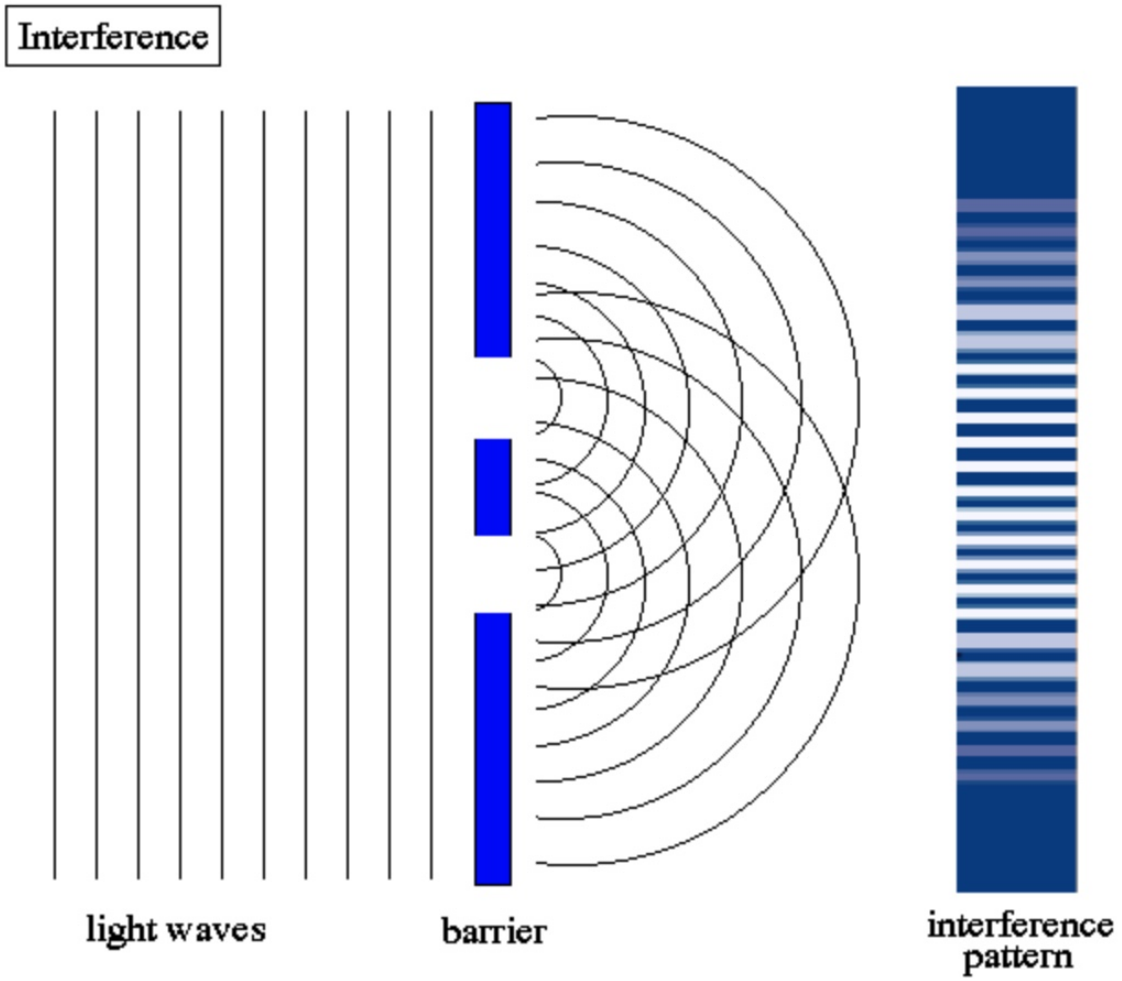

Figure 19: Double slit experiment interference pattern.) at $t = 0.00187, n = 97$.

Results
We simulated how the wave function interacts with a double slit potential in the videos *Double_slit.avi* and *Double_slit_diffraction_pattern.avi*. The two videos plot the results of $\sqrt{\psi\psi*}$ from the same simulation. In the second video we've set all values to the left of the slits to 0 so that the interference pattern would be more prominent.

For this simulation we wanted to mimic the setup of the double slit experiment where a plane wave distribution is incident on the slits. To do so, we defined an intial gaussian distribution centered of $x_0 = 0.5$ and $y_0 = 0.15$ with a really large x width $\delta_x = 0.5$ and thin y width δ_y. Since we want the distribution to hit the potential we defined the x and y momentum/speed to be $p_x = 0$ and $p_y = 100$. This incident wave function can be seen on the right of figure 20. To the left of the same figure we can see the interference pattern. $\sqrt{\psi\psi^*}$ at that same time is re-plotted in figure 21 omitting

Table 8: 2D Double Slit Potential Experiment Parameters

Parameter	**Value**
Initial Condition	$\psi(x, y, 0) = e^{i100y} e^{-((x-0.5)^2/.5^2 + (y-0.15)^2/0.01^2)}$
Potential	Double Slit $V = 10^8$, slit distance $= 0.15$ (centered at $x = 0.5$), slit size $= 0.02$.
Level	9
λ	0.01
t_{max}	0.003

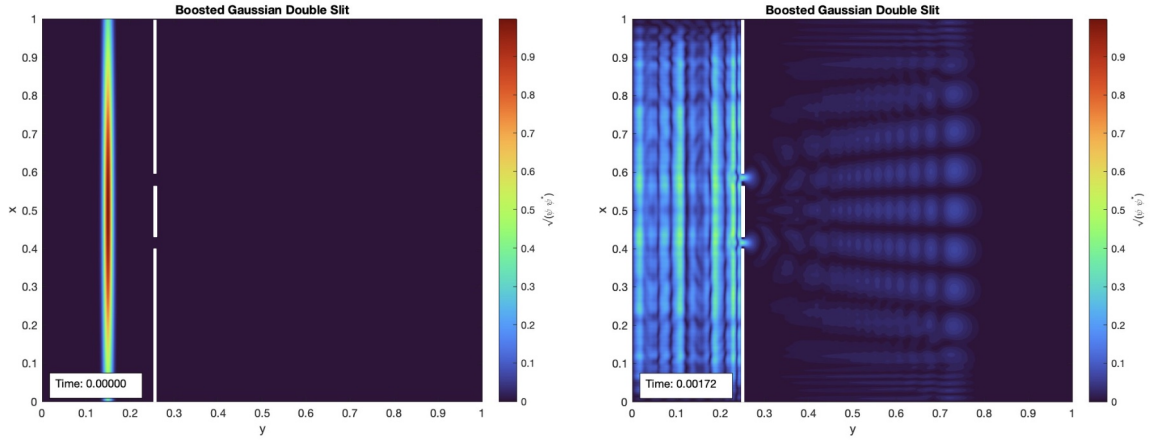

Figure 20: Double slit simulation results. Incident wave form at $t = 0$, $n = 1$ (left) and interference pattern at $t = 0.0$, $n = 89$ (left) at $t = 0.00172, n = 89$ (right).

the values to the left of the potential so that the pattern is more visible. We see that it looks like there is 1 wave source at each slit and the waves interfere constructively and destructively to form the expected interference pattern. The interference pattern is most accurate between $0.2 \leq x \leq 8$ beyond does bounds the pattern becomes altered due to the boundary conditions of the system.

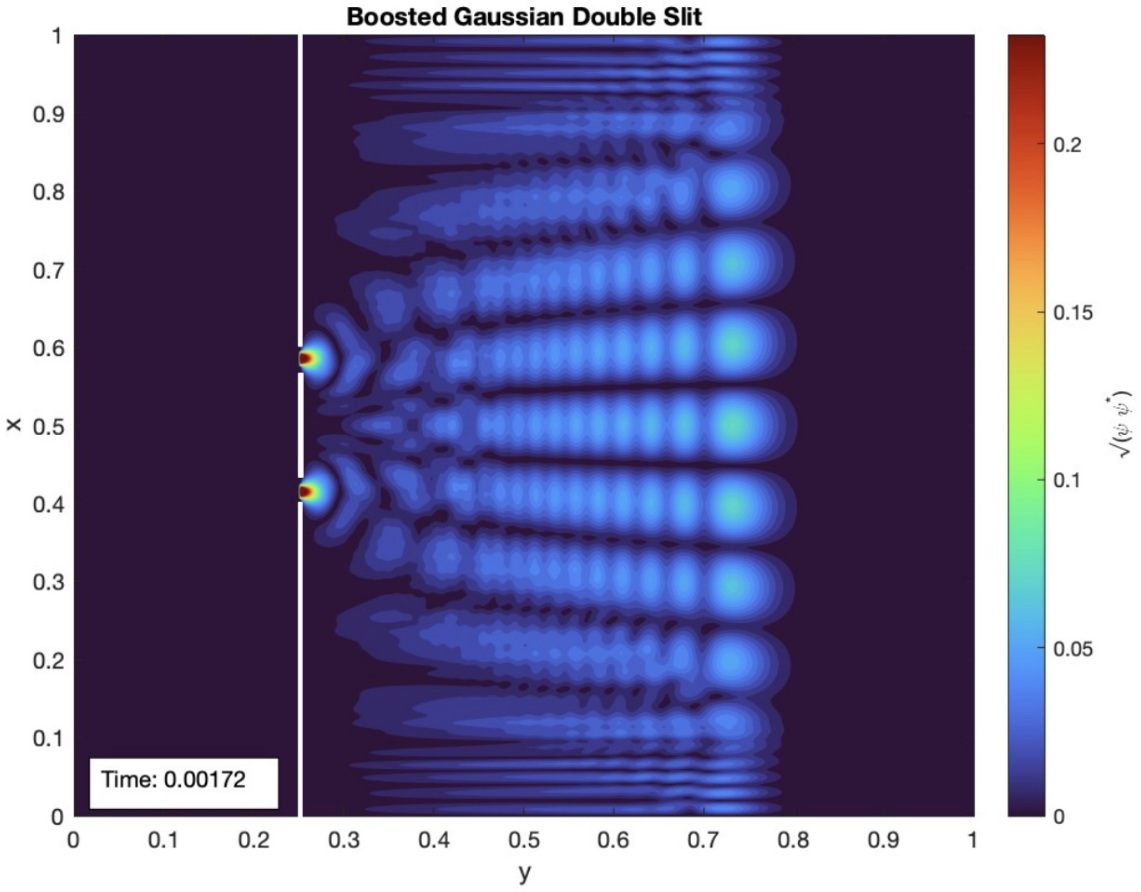

Figure 21: Double slit simulation interference pattern $t = 0.00172, n = 89$ (right).